Journal of
Marine Science and Engineering

MDPI

Article

Bayesian Statistics of Wide-Band Radar Reflections for Oil Spill Detection on Rough Ocean Surface

Bilal Hammoud [1,2,*], Fabien Ndagijimana [2], Ghaleb Faour [3], Hussam Ayad [1] and Jalal Jomaah [1]

[1] Doctoral School of Sciences and Technologies, Lebanese University (LU), 1003 Beirut, Lebanon; hayad@ul.edu.lb (H.A.); jomaah@enserg.fr (J.J.)
[2] Grenoble Electrical Engineering Laboratory, Grenoble Alpes University (UGA), 38031 Grenoble, France; fabien.ndagijimana@univ-grenoble-alpes.fr
[3] National Council of Scientific Research (CNRS-L), Remote Sensing Research Center, 22411 Mansouriyeh, Lebanon; gfaour@cnrs.edu.lb
* Correspondence: bilal.hmd.14@gmail.com

Received: 26 October 2018; Accepted: 18 December 2018; Published: 10 January 2019

Abstract: In this paper, we present a probabilistic approach which uses nadir-looking wide-band radar to detect oil spills on rough ocean surface. The proposed approach combines a single-layer scattering model with Bayesian statistics to evaluate the probability of detection of oil slicks, within a plausible range of thicknesses, on seawater. The difference between several derived detection algorithms is defined in terms of the number of frequencies used (within C-to-X-band ranges), as well as of the number of radar observations. Performance analysis of all three types of detectors (single-, dual- and tri-frequency) is done under different surface-roughness scenarios. Results show that the probability of detecting an oil slick with a given thickness is sensitive to the radar frequency. Multi-frequency detectors prove their ability to overcome the performance of the single- and dual-frequency detectors. Higher probability of detection is obtained when using multiple observations. The roughness of the ocean surface leads to a loss in the reflectivity values, and therefore decreases the performance of the detectors. A possible way to make use of the drone systems in the contingency planning is also presented.

Keywords: oil spill; remote sensing; reflection coefficient; electromagnetic roughness; multi-frequency detector; multiple observations; probability density function; probability of detection; contingency planning

1. Introduction

Enormous applications and industries use petroleum products worldwide, and thus require the presence of petroleum materials on site. This need stresses the necessity of moving petroleum substances using maritime ships or underwater pipelines internationally between different continents and countries. In addition to the intentional petroleum waste spill in sea water, transportation is vulnerable to involuntary oil spills from tanker collisions with rocky shoals, ship accidents and pipeline ruptures [1]. The European Space Agency (ESA) stated that more than 4.5 million tons of oil is the estimate of the annual spill worldwide, where 45% of the amount is due to operative discharges from ships [2]. Oil spills in sea water are one of the major incidents which adversely cause long-term repercussions for the maritime environment. They are happening on a global scale, and their influence on the ecosystem is extremely severe. Oil spills, including gasoline, fuel, crude, and bulk oil, will affect the ecosystem starting from maritime life and ending in the human life and environmental disasters. Marine oil spills can be highly dangerous since wind, waves and currents can scatter a large oil spill over a wide area within a few hours in the open sea. Environmental rules, regulations and strict

operating procedures have been imposed to prevent oil spills, but these measures cannot completely eliminate the risk [3]. Therefore, oil spill detecting and monitoring systems are extremely important in order to react quickly and to limit contamination.

Oil spill detection and monitoring is done with the aid of several techniques and sensors. State-of-the-art sensor technology for oil spill surveillance is listed and described in [4–6]. Infrared sensors are relatively cheap remote-sensing technologies which can be used to detect oil spills. However, thermal radiation from sea weeds appear similar to the radiation arising from the oil which may lead to a false positive result. In addition, infrared sensors require the absence of cloud and heavy fog for good operation [4]. Ultraviolet (UV) sensors cannot detect oil thickness greater than 10 microns. Less UV use is being made for oil spills in today's remote sensing because of the low relevance of thin slicks to oil spill cleanup [6–8]. Microwave radiometer (MWR) is an additional passive sensor that is used for oil spill detection and oil thickness measurements. However, MWR sensors are costly and it is complicated to put them into operation. Microwave radiometer sensors require information about many environmental characteristics and oil properties to accurately detect the oil [4]. There are interferences, and signal differentials may be poor. Currently, microwave is not being used for slick imaging [6].

Radar is a very useful active sensor to detect oil over a large area. Thus, it can be used as a first assessment tool to detect the possible location of an oil spill. SAR (Synthetic Aperture Radar) and SLAR (Side-Looking Airborne Radar) are the two most common types of radar which can be used for oil spill remote sensing [4,9]. Synthetic Aperture Radar is the most widely used sensor on spaceborne platforms for oil spill detection [4]. Imaging SAR systems are off-nadir instruments whose backscattering over the ocean is primarily due to Bragg scattering at relevant incident angles. In [10–13], comparison between different spaceborne and airborne SAR algorithms is done. Synthetic Aperture Radar technique is highly prone to false targets, however, and is limited to a narrow range of wind speeds (approximately 2 to 6 m/s). At winds below this, there are not enough small waves to yield a difference between the oiled area and the sea [3]. At low wind speed it is not possible to distinguish between thick and thin oil slicks. The ocean's slight surface roughness due to very low wind speed (<3 m/s) leads the backscattering to be dominated by the specular component, challenging SAR systems for oil spill detection [12]. Therefore, it would be advantageous to study the radar observations from nadir-looking systems since they cover scenarios that cannot be studied by SAR systems. Being largely independent of surface roughness, the returns from nadir (or near-nadir) systems will benefit from the dominance of the specular scattering and enable detection in very low wind conditions.

Most recent ones are those done remotely using airborne [14,15] and satellite systems [16–21]. Satellites face the limitations of overpass frequency and low spatial resolution [5], whereas airborne systems, despite their high cost due to aircraft dedication, can be used directly when needed for real-time dataset processing [4]. The European Maritime Safety Agency (EMSA) launched in 2016 the need to complement the satellite maritime surveillance systems—that can detect only 25% of pollution accidents—by drones [22]. According to [23], aerial surveillance could be improved significantly by the admission of drones.

According to [7], sensors should provide the following information for oil spill contingency planning:

- *info 1:* the location and spread of an oil spill over a large area,
- *info 2:* the thickness distribution of an oil spill to estimate the quantity of spilled oil,
- *info 3:* a classification of the oil type in order to estimate environmental damage and to take appropriate response activities,
- *info 4:* and timely and valuable information to assist in cleanup operations.

From a system-level perspective, we study the incorporation of both C-band and X-band using remote sensing nadir-looking wide-band radar sensors that can be implemented on drones as oil spill detection systems. The drone-based radar will allow quick assessment of the area where the flag of

possible spills is raised by witnesses. Winds and the ocean's currents may spread the spilled oil to a large area within a short period of time [4], hence the proposed systems will be able to provide the most critical information needed for an effective contingency planning by specifying the location of the oil (*info 1*) and its spread over the ocean. Nevertheless, working as nadir-looking systems will definitely decrease the surface of the scanned area viewed by the radar compared to that scanned by "side-looking" radars. However, parallelization in scanning can be used to cover large area in a critical time. This means that instead of using a single drone with several scans to cover a large area, multiple drones can be used at the same time. Using the radar on drone platforms will be a complementary solution to the satellite systems. Once we have a flag of possible oil spill (due to collision of tankers, or to the rupture of pipelines), the drones can be used to start the scans as tactical-response systems. Afterwards, the satellites can be used for strategic planning by providing the synoptic view of the scene. This will assist later in cleanup operations by providing valuable data as needed (*info 4*). Furthermore, scanning with drones provides high spatial resolution compared to satellite and with a principal advantage of relative low cost compared to dedicated airborne detection systems. With respect to (*info 2*), we proposed in [24] using the same drones systems implementing different algorithms to estimate the thickness of the oil. This information is very important to the effectiveness of oil spill contingency planning because it allows the estimation of the total volume spilled.

We developed in [25,26] dual- and multi-frequency algorithms using only single observations for oil spill detection. The model adopted was a planar multi-layer structure. The ocean surface was assumed to be totally smooth corresponding to scenarios where the wind speed is very low. Performance analysis of the proposed algorithms was presented in [27]. In this journal, we extend the previously proposed approach by applying Bayesian statistics on the reflectivity values evaluated at multiple frequencies and collected with multiple observations. A full derivation of the different algorithms is presented. In addition, the multi-layer structure is no more assumed to be planar. The statistical attributes of the ocean surface are presented. The performance of the detectors is tested under different roughness scenarios. Since the oil properties (*info 3*) are not known during the first stages of an oil spill, we study the effect of this missed information on the overall performance of the proposed algorithms.

2. Methods

2.1. Reflection Coefficient Calculation for the Multi-Layer Planar Structure

From a physical point of view, the problem is considered to be a multi-layer structure where we study the reflection of the electromagnetic waves from the sea layer covered by an oil layer. The electrical properties and the physical characteristics are defined for the layers at the boundaries where interaction with electromagnetic waves occurs.

In our model, we assume that there is an oil slick, with d thickness (in mm), on the top of the sea water surface. An oil spill on the sea surface will dampen the waves and hence reduce the surface roughness. Furthermore, at open ocean space, with low wind speeds (2–6 m/s) which are considered to be optimal for oil spill detection [4], the correlation length of the ocean waves is large and the root-mean-square (rms) height of the capillary waves is very small. Hence, we assume that the multi-layer structure is planar. We consider that this assumption is indeed realistic when the ocean's surface is very smooth due to the very low wind conditions. When the roughness increases, it decreases the reflection measurements made or increases the noise level of the environment.

The relative dielectric constants of the air, oil, and sea water are respectively ε_1, ε_2 and ε_3. The different media are assumed to be non-magnetic. The refractive indices n for the different materials are $n_i = \sqrt{\varepsilon_i}$. The electromagnetic waves are assumed to be normally incident on the ocean surface. We assume that the sea water is deep enough so that we can neglect the radar reflections from the sea-floor. The field reflection coefficients for the first interface (between air and oil) and the second interface (between oil and water) are respectively:

$$\rho_{12} = \frac{n_1 - n_2}{n_1 + n_2}, \tag{1}$$

$$\rho_{23} = \frac{n_2 - n_3}{n_2 + n_3}. \tag{2}$$

Across the boundaries, E is conserved. Using continuity property at these interfaces, the reflectivity (power reflection coefficient) for the three-layer structure is derived in [25] as:

$$R = |\rho|^2 = \frac{\rho_{12}^2 + \rho_{23}^2 + 2\,\rho_{12}\,\rho_{23}\,\cos(2\,\delta)}{1 + \rho_{12}^2\,\rho_{23}^2 + 2\,\rho_{12}\,\rho_{23}\,\cos(2\,\delta)}. \tag{3}$$

The phase shift δ is dependent on the oil-refractive index n_2, the wavelength of the electromagnetic wave λ_0, and the thickness of the oil slick t. It is given by:

$$\delta = \frac{2\,\pi\,f}{c}\,n_2\,t = \frac{2\,\pi}{\lambda_0}\,n_2\,t, \tag{4}$$

where c is the speed of light.

The reflectivity R is a trigonometric function with period T_R that is dependent on the oil-refractive index and the frequency of the electromagnetic wave. The period is expressed as:

$$T_R = \frac{2\,\pi}{\frac{2\,\delta}{t}} = \frac{\pi}{\frac{2\,\pi}{\lambda_0}\,n_2} = \frac{\lambda_0}{2\,\sqrt{\varepsilon_2}}. \tag{5}$$

2.2. Smooth or Rough Surface

Several statistical attributes can be calculated for a random surface [28]. The collection of surface height measurements may be described using standard statistical parameters. The surface height measurements are denoted by $z_{(i,j)}$ in two-dimensional array $N \times N$ collected at a horizontal step-size Δx over an area whose length and width are given by L [29]:

$$z_{(x,y)}(\Delta x, L) \tag{6}$$

with $(x, y) \in [1, ..., N][1, ..., N]$.

Collecting big number of measurements, the height probability density function $p(z)$ can be approximated to one of many well-known distributions such as Gaussian, Exponential, or Rayleigh. For most random surfaces, the probability density function (pdf) looks approximately Gaussian in shape, that is [28,29]

$$p(z) = \frac{1}{\sqrt{2\,\pi s^2}} e^{\frac{-z^2}{2s^2}} \tag{7}$$

where s^2 is the variance of surface heights. With zero-mean distribution, the variance is equal to the standard deviation.

Given $p(z)$, we can calculate several statistical attributes of the random surface, including [28]:

- the height standard deviation s given by

$$s = \sqrt{\int_{-\inf}^{+\inf} z^2 p(z) dz} \tag{8}$$

which is also called the rms-height , and

- the surface correlation function defined by

$$l(\xi) = \frac{\langle z_{(x,y)} z_{(x',y')} \rangle}{s^2} \tag{9}$$

where (x, y) and (x', y') are two locations on the surface, and ξ is the lateral separation between them.

The correlation function $l(\xi)$ is a measure of the degree of correlation between the surface at different locations. The value of the correlation function decreases with ξ. Hence, if the spacing between two locations is greater than a certain distance called the correlation length, we can assume that the heights are considered to be statistically uncorrelated [28].

Electromagnetically, the roughness of a surface is measured relatively to the electromagnetic (EM) wavelength λ. According to [28], for a surface with rms height s, its electromagnetic roughness ks is:

$$ks = \frac{2\pi}{\lambda} s \tag{10}$$

For a perfectly smooth surface (flat surface) with rms height $s = 0$, an incident EM wave is reflected along the specular direction, and the reflected power is related to the incident power by the reflectivity formula given in Equation (3).

The component of the scattering pattern of the perfectly smooth surface consists of only a coherent component. If the surface is rough with ks, the scattering pattern will also include a non-coherent component along all other directions. In that case, the reflectivity along the specular direction will be noted as the coherent reflectivity R_{coh}, expressed as

$$R_{coh} = R\, e^{-4\psi^2} \tag{11}$$

where

$$\psi = ks \cos(\theta_i) = \frac{2\pi}{\lambda} s \cos(\theta_i) \tag{12}$$

with θ_i being the incident angle of the EM wave to the interfaces.

With respect to the oil spill problem, according to [11,13], an oil spill on the sea surface dampens the waves and hence reduces the roughness of the surface. Furthermore, at open ocean space, with very low wind speed (<2–3 m/s) which are considered to be optimal for oil spill detection [4], the correlation length of the ocean waves is large and the rms height s of the capillary waves is very small. Hence, the electromagnetic roughness ks is negligible and all interfaces are assumed to be planar.

When the variation of the ocean waves increases due to higher wind speed, the electromagnetic roughness increases respectively with the rms height s. Therefore, the surface is not considered to be totally planar anymore, and its variation will affect its level of roughness. Depending on the electromagnetic roughness factor, the surface can be described to be planar ($ks = 0$), relatively smooth ($ks = 0.2$) or extremely rough ($ks = 2$). The effect of the electromagnetic roughness on the reflectivity value is displayed in Figure 1 [28].

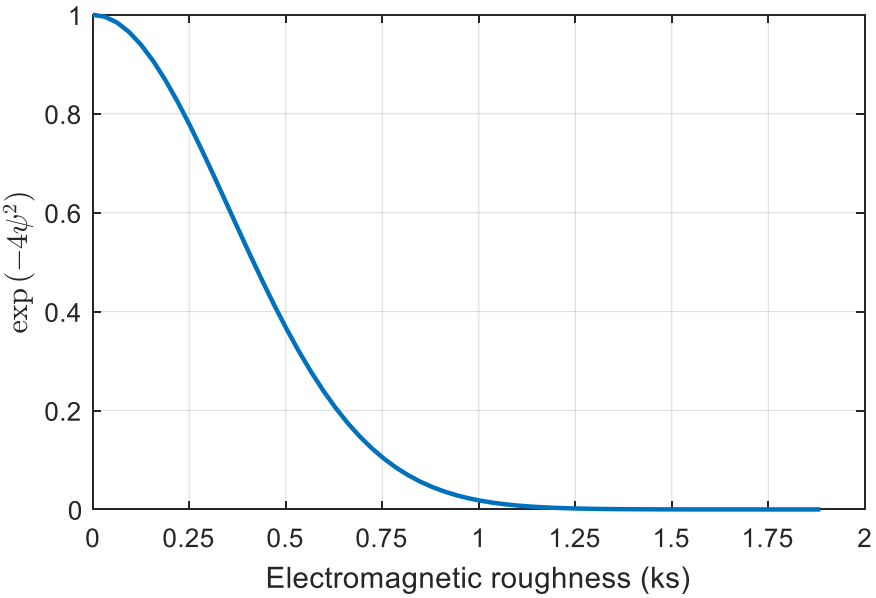

Figure 1. Effect of the electromagnetic roughness on the reflectivity value.

2.3. Detection Algorithms

From the mathematical perspective, the detector algorithms use the statistical characterization of the reflectivity values and its distribution under different oil thicknesses in order to obtain a final decision whether oil exists or not. These reflectivity values are assumed to be independent events. Any previous knowledge about the existence or absence of oil in the surface scanned should be taken into consideration to weight the probability of the decision in the detector block. Nevertheless, without any previous knowledge about the spill situation, the detector decision will be totally based on the statistics of the calculated power reflection ratio.

Let "o, w" be the events indicating the presence of the oil slick and the water, respectively. Let R be the event representing the reflectivity value(s) measured. R could represent one or more reflectivity values repeated at the same frequency or at different frequencies. In all cases, these reflectivity values are assumed to be uncorrelated in time domain (at multiple observations) and in frequency domain (at multiple frequency measurements). The difference between these cases will be studied in the following subsections. With "$\cdot$" being the numerical multiplication, the probability of oil presence and absence given R are respectively

$$Pr(o|R) = \frac{Pr(o \cap R)}{Pr(R)} = \frac{Pr(R|o) \cdot Pr(o)}{Pr(R)} \tag{13}$$

$$Pr(w|R) = \frac{Pr(w \cap R)}{Pr(R)} = \frac{Pr(R|w) \cdot Pr(w)}{Pr(R)} \tag{14}$$

Without any previous knowledge about the spill situation, i.e., with $Pr(o) = Pr(w) = 50\%$, the ratio of probabilities of oil presence to water presence is given by

$$\frac{Pr(o|R)}{Pr(w|R)} = \frac{Pr(R|o) \cdot Pr(o)}{Pr(R|w) \cdot Pr(w)} = \frac{Pr(R|o)}{Pr(R|w)}. \tag{15}$$

The probability of obtaining a measured reflectivity value given that the oil exists is evaluated using the corresponding pdf. Similarly, the probability of obtaining the same reflectivity value given that the water exists is evaluated. If the ratio in (15) gives a result greater than unity, the decision will indicate the oil existence.

2.3.1. Single Observation at Multiple Frequencies

If R in (15) represents single observations of reflectivity measured at different frequencies (up to I total frequencies), then we can express it as

$$R = R_{f_1}, R_{f_2}, ...R_{f_I} \tag{16}$$

Replacing (16) in (15), we obtain

$$\begin{aligned} \frac{Pr(o|R)}{Pr(w|R)} &= \frac{Pr(R_{f_1}, R_{f_2}, ...R_{f_I}|o)}{Pr(R_{f_1}, R_{f_2}, ...R_{f_I}|w)} \\ &= \frac{Pr(R_{f_1}|o) \cdot \ \ldots \ \cdot Pr(R_{f_I}|o)}{Pr(R_{f_1}|w) \cdot \ldots \cdot Pr(R_{f_I}|w)} \\ &= \frac{Pr(R_{f_i}, R_{f_j}, ..|o)}{Pr(R_{f_i}, R_{f_j}, ..|w)} \cdot \frac{Pr(o)}{Pr(w)} \\ &= \frac{\prod_i Pr(R_{f_i}|o)}{\prod_i Pr(R_{f_i}|w)} \\ &= \prod_i \frac{Pr(R_{f_i}|o)}{Pr(R_{f_i}|w)} \end{aligned} \tag{17}$$

2.3.2. Multiple Observations at Single Frequency

If R in (15) represents multiple observations (up to M total observations) of reflectivity measured at single frequency, then we can express it as

$$R = R_{f_1}^{(1)}, R_{f_1}^{(2)}, ...R_{f_1}^{(M)} \tag{18}$$

Replacing (18) in (15), we obtain

$$\begin{aligned} \frac{Pr(o|R)}{Pr(w|R)} &= \frac{Pr(R_{f_1}^{(1)}, R_{f_1}^{(2)}, ...R_{f_1}^{(M)}|o)}{Pr(R_{f_1}^{(1)}, R_{f_1}^{(2)}, ...R_{f_1}^{(M)}|w)} \\ &= \frac{Pr(R_{f_1}^{(1)}|o) \cdot \ \ldots \ \cdot Pr(R_{f_1}^{(M)}|o)}{Pr(R_{f_1}^{(1)}|w) \cdot \ldots \cdot Pr(R_{f_1}^{(M)}|w)} \\ &= \frac{\prod_m Pr(R_{f_1}^{(m)}|o)}{\prod_m Pr(R_{f_1}^{(m)}|w)} \\ &= \prod_m \frac{Pr(R_{f_1}^{(m)}|o)}{Pr(R_{f_1}^{(m)}|w)} \end{aligned} \tag{19}$$

2.3.3. Multiple Observations and Multiple Frequencies

If R in (15) represents multiple observations (up to M total observations) of reflectivity measured at multiple frequencies (up to I total frequencies) , then we can express it as

$$R = R_{f_1}^{(1)}, ..., R_{f_1}^{(M)}, R_{f_2}^{(1)}, ..., R_{f_2}^{(M)}, ..., R_{f_I}^{(1)}, ..., R_{f_I}^{(M)} \tag{20}$$

Replacing (20) in (15), we obtain

$$\begin{aligned}
\frac{Pr(o|R)}{Pr(w|R)} &= \frac{Pr(R_{f_1}^{(1)},...,R_{f_1}^{(M)},R_{f_2}^{(1)},...,R_{f_I}^{(M)}|o)}{Pr(R_{f_1}^{(1)},...,R_{f_1}^{(M)},R_{f_2}^{(1)},...,R_{f_I}^{(M)}|w)} \\
&= \frac{Pr(R_{f_1}^{(1)}|o)\cdot\ \ldots\ \cdot Pr(R_{f_1}^{(M)}|o)}{Pr(R_{f_1}^{(1)}|w)\cdot\ldots\cdot Pr(R_{f_1}^{(M)}|w)} \\
&\quad\times\frac{Pr(R_{f_2}^{(1)}|o)\cdot\ \ldots\ \cdot Pr(R_{f_2}^{(M)}|o)}{Pr(R_{f_2}^{(1)}|w)\cdot\ldots\cdot Pr(R_{f_2}^{(M)}|w)} \\
&\quad\times\ldots \\
&\quad\times\frac{Pr(R_{f_I}^{(1)}|o)\cdot\ \ldots\ \cdot Pr(R_{f_I}^{(M)}|o)}{Pr(R_{f_I}^{(1)}|w)\cdot\ldots\cdot Pr(R_{f_I}^{(M)}|w)} \\
&= \frac{\prod_m Pr(R_{f_1}^{(m)}|o)}{\prod_m Pr(R_{f_1}^{(m)}|w)}\times\ldots\frac{\prod_m Pr(R_{f_I}^{(m)}|o)}{\prod_m Pr(R_{f_I}^{(m)}|w)} \\
&= \prod_i\prod_m \frac{Pr(R_{f_i}^{(m)}|o)}{Pr(R_{f_i}^{(m)}|w)}
\end{aligned} \tag{21}$$

3. Results and Discussion

3.1. Simulation Setup

Probability of detection calculations are performed using Monte Carlo Simulations in MATLAB. The dielectric constant of the air is $\varepsilon_1 = 1$. The dielectric constant of the thick oil is assumed to be real $\varepsilon_2 = 3$ (the imaginary part of order 0.01 j can be neglected without affecting the results). Sea water dielectric constant, ε_3, is function of the water temperature t_w, water salinity s_w and the frequency of the electromagnetic signal used. For its calculation, we use the model mentioned in [28] with $t_w = 20^\circ$ C and $s_w = 35$ ppt. The noise variance in the system is considered to be additive white Gaussian (AWG) in linear scale, with variance of $\sigma^2 = 0.02$.

3.2. Reflectivity Behavior with Smooth and Rough Surfaces

Figure 2 shows the reflectivity values (coherent component) calculated from the planar multi-layer structure versus the oil thickness, under different electromagnetic roughness ($ks = 0$, 0.2 and 0.5). The plot of $R_{coh,w}$ is simply a copy of the value obtained at $d = 0$ mm at the given frequency. For totally smooth surfaces, the plot of $R_{coh,o}$ at 4 GHz is almost monotonically decreasing in the range (0–10 mm). It has a very small slope at small thickness values (0–3 mm), but this slope increases with the increase of the oil slick thickness (3–7 mm). At some thicknesses, any error in the power reflectivity measurements at 4 GHz would mislead the oil detection due to the very small variation between $R_{coh,o}$ and $R_{coh,w}$.

The variation of the reflectivity values at 12 GHz is quite high for consecutive values of thicknesses. This variation allows the oil detection for small thicknesses (1–3 mm). As discussed in Equation (5), the reflectivity is a trigonometric function and has a cyclic behavior. This is observed clearly at $f = 12$ GHz; the reflectivity repeats every 7.2 mm. Due to the cyclic behavior, many thickness values give the same reflectivity value leading to false interpretations. Therefore, it is important to use more than one frequency to improve the detection. When the electromagnetic roughness of the surfaces increases, the reflectivity values decrease as presented in Equation (11). Increasing the surface roughness ks from 0.2 to 0.5 leads approximately to 4 dB loss in the reflectivity.

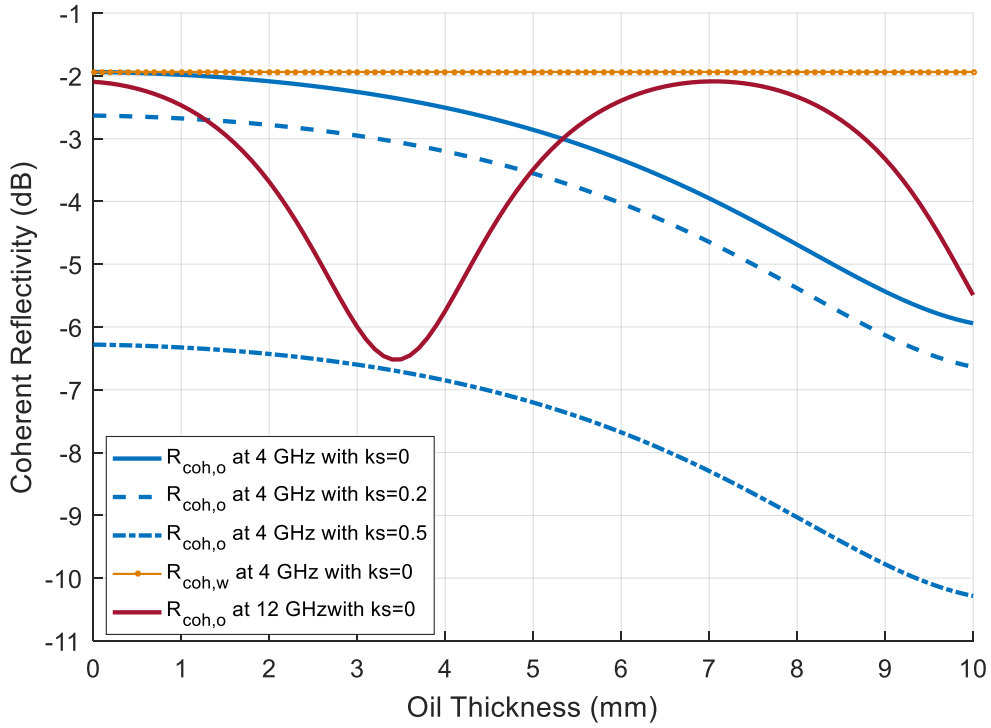

Figure 2. Comparison between the reflectivity values (in dB) versus the oil thickness (in mm) at 4 GHz and 12 GHz for different roughness scenarios. R_o and R_w in each graph represents the oil and water reflectivity values, respectively.

3.3. Effect of the Oil Properties on the Performance of the Single-Frequency Detectors

In real scenarios, when oil spill takes place, it is not always the case that the oil type is well known and defined. This rises the following question from system-monitoring aspect: Does the absence of the exact value of the oil property affects the reflectivity values? To answer this, Figure 3 presents the reflectivity values for different relative dielectric constants of the oil ($\varepsilon_2 = 2.9, 3$ and 3.3) at two frequencies (4 and 12) GHz. At 4 GHz, the difference in the relative dielectric constant values does not modify the reflectivity values at (0–3) mm. However, for higher thickness values, the reflectivities start to change for different dielectric constants. At 4 GHz, the difference between the reflectivities when $\varepsilon_2 = 2.9$ and $\varepsilon_2 = 3.3$ reaches approximately 1 dB at around 7.8 mm. At 12 GHz, the difference is high at around 3.5 mm, decreases to null at 7.8 mm and increases again to 2 dB at 10 mm. Now, we know that the oil type slightly affects the reflectivity value, but more importantly, is it the case for the performance of the detectors?

Figure 4 compares between the probability of detection versus the oil thickness (in mm) for different single-frequency detectors with single scan ($M = 1$) and variant oil properties. Using the detector with single observation at 4 GHz, the probability of oil detection increases with the oil thickness from 51% to 70%. At 8 GHz, the detector records highest detection of 69% at 5 mm but it fails for thickness ranges (1–2 mm) and (8.5–10 mm) recording a value smaller than 55%. At 12 GHz, the detector fails at 1 mm and between (6–8 mm), where the higher detection occurs at 3.5 mm. The results for all these single-frequency detectors (with single observation) validate the reflectivity behavior explained previously in Figure 2.

The effect of the variation in the reflectivity values, due to the variation of the oil properties, in the performance of the single-frequency detectors is also presented in Figure 4. From the obtained results, we notice that although at different thickness values there exists some noticeable difference in the reflectivity values at the same frequency for different dielectric constants (as shown in Figure 3), but these variations do not affect the performance of the detectors more than 2%. Therefore, even when monitoring an oil spill, the proposed algorithms can be used with an approximate value of the oil

permittivity without affecting the performance of the technique on the detection. This analysis is highly useful for the monitoring system because it defines the vulnerability of the drone systems against the absence of some information about the oil properties that are not be present during tactical response.

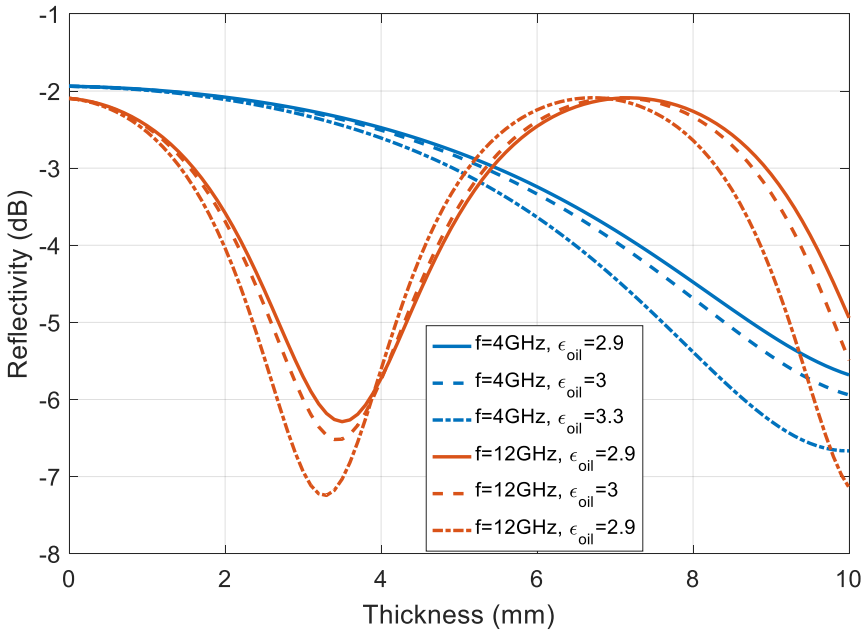

Figure 3. Reflectivity R (in dB) versus oil thickness (in mm) at different frequencies (4 GHz, and 12 GHz) and different oil dielectric constants. The electromagnetic roughness is $ks = 0.5$.

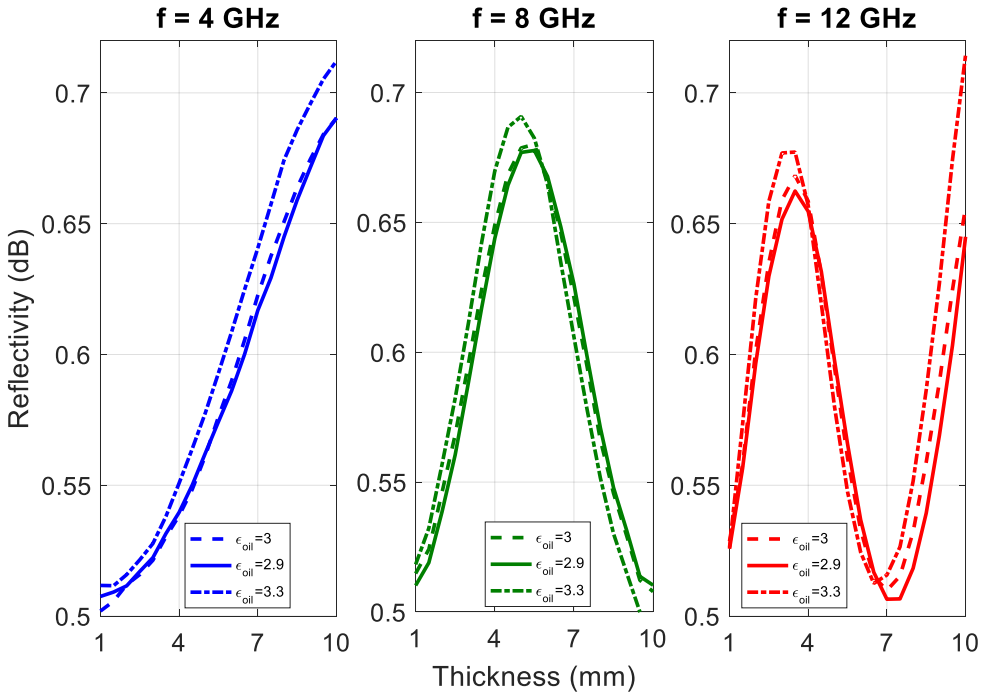

Figure 4. Comparison between the probability of detection versus the oil thickness (in mm) for single-frequency detectors at 4 GHz, 8 GHz and 12 GHz, using single observation ($M = 1$) and different oil properties. The electromagnetic roughness is $ks = 0.5$.

3.4. Performance Analysis of the Multi-Frequency Detectors

Figure 5 compares between the probability of detection versus the oil thickness (in mm) for different single-frequency detectors when the number of observations used by the detectors is varied up to 5. The electromagnetic roughness of the surface is 0.5. The performance of all detectors improves when the number of observations increases from 1 to 5. Using many observations for the detection reduces the AWG noise. However, no improvement is recorded for thickness values equal to multiple of wavelengths. Therefore, even when increasing the number of observations to reduce the effect of the noise, there are still some thickness ranges where the decision is totally wrong. With the use of one frequency, it is not possible to cover all the possible range of thickness values because of the periodicity of the reflectivity. The reflectivity's cyclic behavior highlights the need to use multiple frequencies to achieve accurate decision about the oil spill situation.

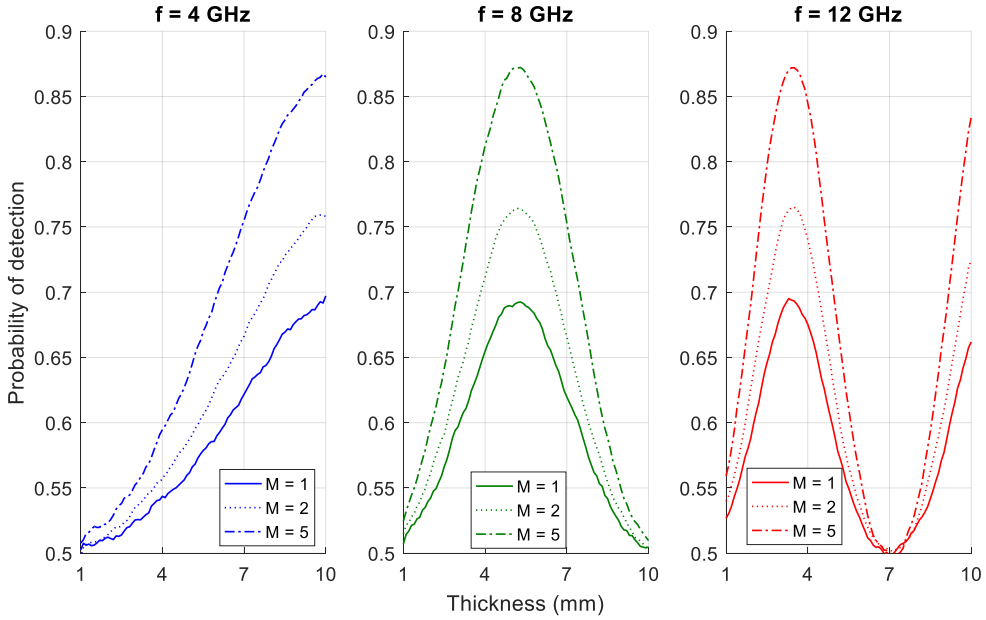

Figure 5. Comparison between the probability of detection versus the oil thickness (in mm) for single-frequency detectors at 4 GHz, 8 GHz and 12 GHz, using single observation ($M = 1$) and multiple observations ($M = 2$ and $M = 5$), with electromagnetic roughness $ks = 0.5$.

Figure 6 compares the probability of detection for different single- and dual-frequency detectors under different surface-roughness scenarios. Using more than one frequency in the detector increases the range of thicknesses over which the detection is correct and omits to a certain extent the drawbacks of the reflectivity cyclic behavior. When combining 4 GHz with 8 GHz, the probability of detection increases to more than 70% for any thickness value exceeding 4.5 mm. Using more observations ($M = 3$ and 5), the dual-frequency detectors performs respectively around 10% and 15% better than using single observation only. The performance of the detection is much efficient when the surface is planar. It is evaluated to be higher than 75% for thickness values greater than 2 mm when $M = 5$. The probability of detection generally improves for a larger number of scans M because the noise will be averaged out. However, with dual-frequency detectors, the probability of detection in the low frequency range is still low. What if we increase the number of frequencies used when scanning?

Figure 7 shows the effect of increasing the number of frequencies on the performance of the detectors. For planar surfaces, the tri-frequency detector using the combination of (4 GHz, 6 GHz and 8 GHz) shows better performance than the combination of (4 GHz, 8 GHz and 12 GHz) in high thickness ranges. The cyclic behavior of the reflectivity at 12 GHz leads to the 8% drop witnessed at 8.5 mm. However, its slope is steepest than the slope of the reflectivity at 6 GHz. This explains the 5–15% less efficiency at low thickness values 1–4 mm.

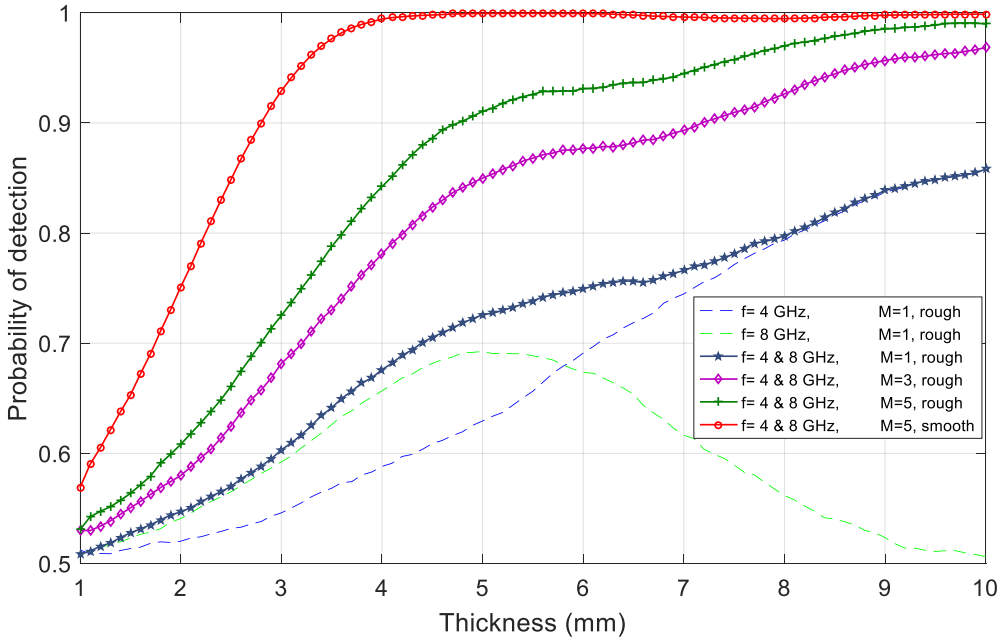

Figure 6. Comparison between the probability of detection versus the oil thickness (in mm) for different detector algorithms: single-frequency detectors at 4 GHz and 8 GHz, and dual-frequency detectors using combinations of these frequencies, for different surface-roughness scenarios.

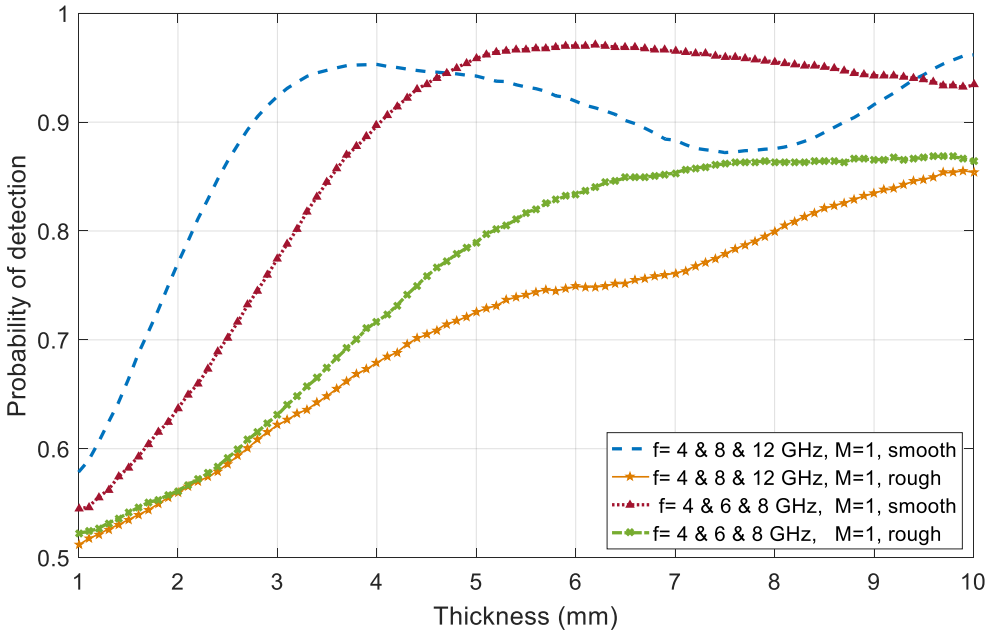

Figure 7. Comparison between the probability of detection versus the oil thickness (in mm) using different multi-frequency detectors for smooth and rough surfaces.

Higher frequencies witness more electromagnetic loss at the same rms height (s) of the surface. Therefore, it would be more advantageous to use lower frequencies when the ocean surface is rough. For electromagnetic roughness $ks = 0.5$, the loss of the reflectivity at 12 GHz is much higher than the loss at 6 GHz. For that reason, the tri-frequency detector that uses 6 GHz instead of 12 GHz gives better performance over all the possible thickness values. By increasing the number of scans, more benefit can be achieved at low thickness values.

Overall, based on the previous obtained results, we can propose the following plan using drone systems for oil spill detection:

1. Receiving alarm for possible oil spill (witnesses, underwater pipelines ruptures, collisions of tankers, etc.)
    - Send multiple drones to test the candidate scene.
    - The drones should use wide-band radar to collect several measurements at different frequencies in each scan.
    - Depending on the weather conditions and the ocean's waves, scan M times the scene to reduce the effect of the noise on the collected measurements as needed.
    - Data collected should be transmitted directly to base stations for post-processing.
2. Apply the detection algorithms on the collected data and analyze it. If the probability of detection exceeds the threshold set by the persons in charge, launch the oil spill alarm and the need to start the contingency plan.
3. Apply the oil thickness estimation algorithms [24] on the collected data to estimate the severity of the spill. High values (>1 mm) indicate the need for quick intervention because the oil slick will be considered to be "thick" and "heavy", and it will persist for a long period of time [4].
4. Use the satellite systems to provide a synoptic view of the scene during the upcoming days to track the spill.
5. Once the contingency plan is started, make use of other sensors to get all other needed information more accurately (for example, the large-size and weight fluoro-sensor can be used to identify the oil type [4].)

4. Conclusions

In this paper, we present a new probabilistic approach using wide-band radar for drone-based oil spill detection applications. We derived multi-frequency algorithms that use the statistical characterization of the power reflectivity and its distribution under various oil thicknesses and electromagnetic wave frequencies. We first introduce multi-frequency single-observation detector that uses single measurement of power reflection coefficient at different frequencies. Then, we present the single-frequency multiple-observations detector that uses multiple measurements of power reflection coefficients over several scanning for the sea area under study. We finally derive the multi-frequency multiple-observations detector that uses different frequencies at the same time and repetitively to provide a final decision about oil spill presence or absence. Performance analysis of all three types of detectors is done. Results show the inability of the single-frequency detectors to effectively distinguish between oil slicks and water for the total range of possible thicknesses. Nevertheless, increasing the number of observations leads to an increase in the effectiveness of the detectors. Dual-frequency and tri-frequency detectors prove their ability to overcome the drawbacks of the single-frequency detector by providing accurate detection especially for multiple observations. The performance of these detectors is reduced when the roughness of the ocean surface due to winds increases. The proposed algorithms can be implemented on nadir-looking systems such as the drones to be complementary systems for oil spill detection. Using multiple drones at the same time allow for quick intervention and real-time data collection for post-processing. During the early stages of a possible oil spill, the drone systems act as tactical-response systems complementing the large-scale view obtained by satellite systems. Once the spill is confirmed, the drones can track the spill using the high spatial resolution feature provided by the wide-band radars.

Author Contributions: Conceptualization, methodology, investigation, and writing of the paper, B.H.; results discussion, F.N.; funding acquisition, F.N. and Gh.F.; supervision, F.N., H.A. and J.J.

Funding: This work was supported by the National Council of Research at Lebanon (CNRS-L).

Conflicts of Interest: The authors declare no conflict of interest.

References

1. Alpers, W. Remote sensing of oil spills. In Proceedings of the Maritime Disaster Management Symposium, Dhahran, Saudi Arabia, 19–23 January 2002; pp. 19–23.
2. Oil Pollution Monitoring. Remote Sensing Exploitation Division. ESRIN—European Space Agency (ESA). p. 2. Available online: http://www.esa.int/esapub/br/br128/br128_1.pdf (accessed on 18 December 2018).
3. Fingas, M. *The Basics of Oil Spill Cleanup*; CRC Press: Boca Raton, FL, USA, 2012.
4. Jha, M.N.; Levy, J.; Gao, Y. Advances in remote sensing for oil spill disaster management: State-of-the-art sensors technology for oil spill surveillance. *Sensors* **2008**, *8*, 236–255. [CrossRef] [PubMed]
5. Leifer, I.; Lehr, W.J.; Simecek-Beatty, D.; Bradley, E.; Clark, R.; Dennison, P.; Hu, Y.; Matheson, S.; Jones, C.E.; Holt, B.; et al. State of the art satellite and airborne marine oil spill remote sensing: Application to the BP Deepwater Horizon oil spill. *Remote Sens. Environ.* **2012**, *124*, 185–209. [CrossRef]
6. Fingas, M.; Brown, C.E. A review of oil spill remote sensing. *Sensors* **2017**, *18*, 91. [CrossRef] [PubMed]
7. Grüner, K.; Reuter, R.; Smid, H. A new sensor system for airborne measurements of maritime pollution and of hydrographic parameters. *GeoJournal* **1991**, *24*, 103–117. [CrossRef]
8. Yin, D.; Huang, X.; Qian, W.; Huang, X.; Li, Y.; Feng, Q. Airborne validation of a new-style ultraviolet push-broom camera for ocean oil spill pollution surveillance. Remote Sensing of the Ocean, Sea Ice, and Large Water Regions 2010. *Int. Soc. Opt. Photonics* **2010**, *7825*, 78250I.
9. Fingas, M.F.; Brown, C.E. Review of oil spill remote sensing. *Spill Sci. Technol. Bull.* **1997**, *4*, 199–208. [CrossRef]
10. Yang, C.S.; Kim, Y.S.; Ouchi, K.; Na, J.H. Comparison with L-, C-, and X-band real SAR images and simulation SAR images of spilled oil on sea surface. In Proceedings of the 2009 IEEE International Geoscience and Remote Sensing Symposium, IGARSS 2009, Cape Town, South Africa, 12–17 July 2009; Volume 4, pp. IV–673.
11. Skrunes, S.; Brekke, C.; Eltoft, T. Oil spill characterization with multi-polarization C-and X-band SAR. In Proceedings of the 2012 IEEE International Geoscience and Remote Sensing Symposium (IGARSS), Munich, Germany, 22–27 July 2012; pp. 5117–5120.
12. Skrunes, S.; Brekke, C.; Eltoft, T.; Kudryavtsev, V. Comparing near-coincident C-and X-band SAR acquisitions of marine oil spills. *IEEE Trans. Geosci. Remote Sens.* **2015**, *53*, 1958–1975. [CrossRef]
13. Marzialetti, P.; Laneve, G. Oil spill monitoring on water surfaces by radar L, C and X band SAR imagery: A comparison of relevant characteristics. In Proceedings of the 2016 IEEE International Geoscience and Remote Sensing Symposium (IGARSS), Beijing, China, 10–15 July 2016; pp. 7715–7717.
14. Collins, M.J.; Denbina, M.; Minchew, B.; Jones, C.E.; Holt, B. On the use of simulated airborne compact polarimetric SAR for characterizing oil–water mixing of the deepwater horizon oil spill. *IEEE J. Sel. Top. Appl. Earth Obs. Remote Sens.* **2015**, *8*, 1062–1077. [CrossRef]
15. Hensley, S.; Jones, C.; Lou, Y. Prospects for operational use of airborne polarimetric SAR for disaster response and management. In Proceedings of the 2012 IEEE International Geoscience and Remote Sensing Symposium (IGARSS), Munich, Germany, 22–27 July 2012; pp. 103–106.
16. Laneve, G.; Luciani, R. Developing a satellite optical sensor based automatic system for detecting and monitoring oil spills. In Proceedings of the 2015 IEEE 15th International Conference on Environment and Electrical Engineering (EEEIC), Rome, Italy, 10–13 July 2015; pp. 1653–1658.
17. Dan, W.; Jifeng, S.; Yongzhi, Z.; Pu, Z. Application of the marine oil spill surveillance by satellite remote sensing. In Proceedings of the 2009 International Conference on Environmental Science and Information Application Technology, Wuhan, China, 4–5 July 2009; Volume 1, pp. 505–508.
18. Rocca, F. Remote sensing from space for oil exploration. In Proceedings of the 2015 IEEE International Geoscience and Remote Sensing Symposium (IGARSS), Milan, Italy, 26–31 July 2015; pp. 2876–2879.
19. Minchew, B.; Jones, C.E.; Holt, B. Polarimetric analysis of backscatter from the Deepwater Horizon oil spill using L-band synthetic aperture radar. *IEEE Trans. Geosci. Remote Sens.* **2012**, *50*, 3812–3830. [CrossRef]
20. Bayındır, C.; Frost, J.D.; Barnes, C.F. Assessment and Enhancement of SAR Noncoherent Change Detection of Sea-Surface Oil Spills. *IEEE J. Ocean. Eng.* **2018**, *43*, 211–220. [CrossRef]
21. Xu, L.; Wong, A.; Clausi, D.A. An Enhanced Probabilistic Posterior Sampling Approach for Synthesizing SAR Imagery With Sea Ice and Oil Spills. *IEEE Geosci. Remote Sens. Lett.* **2017**, *14*, 188–192. [CrossRef]

22. Lecomte, E. En Fevrier 2017, des Drones vont Traquer la Pollution Maritime. 2017. Available online: https://www.sciencesetavenir.fr/high-tech/drones/en-fevrier-2017-des-drones-vont-traquer-la-pollution-maritime_109732 (accessed on 1 January 2017).
23. Kirkos, G.; Zodiatis, G.; Loizides, L.; Ioannou, M. Oil Pollution in the Waters of Cyprus. In *The Handbook of Environmental Chemistry*; Springer: Berlin/Heidelberg, Germang, 2017; doi:10.1007/698_2017_49.
24. Hammoud, B.; Ayad, H.; Fadlallah, M.; Jomaah, J.; Ndagijimana, F.; Faour, G. Oil Thickness Estimation Using Single-and Dual-Frequency Maximum-Likelihood Approach. In Proceedings of the 2018 International Conference on High Performance Computing & Simulation (HPCS), Orleans, France, 16–20 July 2018; pp. 65–68.
25. Hammoud, B.; Mazeh, F.; Jomaa, K.; Ayad, H.; Ndadijimana, F.; Faour, G.; Fadlallah, M.; Jomaah, J. Multi-Frequency Approach for Oil Spill Remote Sensing Detection. In Proceedings of the 2017 International Conference on High Performance Computing & Simulation (HPCS), Genoa, Italy, 17–21 July 2017; pp. 295–299.
26. Hammoud, B.; Mazeh, F.; Jomaa, K.; Ayad, H.; Ndagijimana, F.; Faour, G.; Jomaah, J. Dual-frequency oil spill detection algorithm. In Proceedings of the 2017 Computing and Electromagnetics International Workshop (CEM), Barcelona, Spain, 21–24 June 2017; pp. 27–28.
27. Hammoud, B.; Faour, G.; Ayad, H.; Ndagijimana, F.; Jomaah, J. Performance Analysis of Detector Algorithms Using Drone-Based Radar Systems for Oil Spill Detection. *Multidiscip. Digit. Publ. Inst. Proc.* **2018**, *2*, 370. [CrossRef]
28. Ulaby, F.T.; Long, D.G.; Blackwell, W.J.; Elachi, C.; Fung, A.K.; Ruf, C.; Sarabandi, K.; Zebker, H.A.; Van Zyl, J. *Microwave Radar and Radiometric Remote Sensing*; University of Michigan Press: Ann Arbor, MI, USA, 2014; Volume 4
29. Campbell, B.A. *Radar Remote Sensing of Planetary Surfaces*; Cambridge University Press: Cambridge, UK, 2002.